The Astrophysical Journal, 706:L17–L21, 2009 November 20 doi:10.1088/0004-637X/706/1/L17

STATISTICS OF FLARES SWEEPING ACROSS SUNSPOTS

Leping Li and Jun Zhang
Key Laboratory of Solar Activity, National Astronomical Observatories, Chinese Academy of Sciences, Beijing 100012, China; lepingli@ourstar.bao.ac.cn, zjun@ourstar.bao.ac.cn
Received 2009 July 2; accepted 2009 September 29; published 2009 October 28

ABSTRACT

Flare ribbons are always dynamic and sometimes sweep across sunspots. After examining 588 (513 M-class and 75 X-class) flare events observed by the *TRACE* satellite and the *Hinode*/Solar Optical Telescope from 1998 May to 2009 May, we choose the event displaying one of the flare ribbons that completely sweeps across the umbra of a main sunspot of the corresponding active region, and finally obtain 20 (7 X-class and 13 M-class) events as our sample. In each event, we define the main sunspot completely swept across by the flare ribbon as the A-sunspot and its nearby opposite polarity sunspot as the B-sunspot. Observations show that the A-sunspot is a following polarity sunspot in 18 events and displays flux emergence in 13 cases. All of the B-sunspots are relatively simple, exhibiting either one main sunspot or one main sunspot and several small neighboring sunspots (pores). In two days prior to the flare occurrence, the A-sunspot rotates in all the cases, while the B-sunspot rotates in 19 events. The total rotating angle of the A-sunspot and B-sunspot rotates is 193° on average, and the rotating directions are the same in 12 events. In all cases; the A-sunspot and B-sunspot manifest shear motions with an average shearing angle of 28°.5, and in 14 cases, the shearing direction is opposite to the rotating direction of the A-sunspot. We suggest that the emergence, the rotation, and the shear motions of the A-sunspot and B-sunspot result in the phenomenon that flare ribbons sweep across sunspots completely.

Key words: Sun: flares – Sun: magnetic fields – sunspots – Sun: UV radiation

1. INTRODUCTION

Solar flares are one of the most spectacular phenomena in solar physics. They are sudden brightenings in the solar atmosphere and consist of a number of components including post-flare loops (Li & Zhang 2009a), flare ribbons (Isobe et al. 2002, 2007; Asai et al. 2004), etc. The flare ribbons are located on either side of the magnetic neutral line, have magnetic polarities opposite to each other, and move apart during the process of the flare. Based on the CSHKP magnetic reconnection model (Carmichael 1964; Sturrock 1966; Hirayama 1974; Kopp & Pneuman 1976), the flare ribbons are caused by the precipitation of nonthermal particles and/or the effect of thermal conduction, which are produced after magnetic field lines reconnect in the corona. At successive reconnections, the reconnection points (X-points) move upward, and therefore, newly reconnected field lines have their footpoints further out than the footpoints of the field lines that have already reconnected, which leads us to recognize the "apparent" separation motion of the flare ribbons. The separation of the flare ribbons has been used to estimate the electric field in the reconnecting current sheet (e.g., Qiu et al. 2002; Asai et al. 2004) and also the coronal magnetic field strength and the reconnection rate (e.g., Isobe et al. 2002; Li & Zhang 2009b). As we all know, the separation of the flare ribbons generally stop at the edge of the sunspots. However, in some flare events, flare ribbons sweep across the main sunspot of the flare source region completely.

In this Letter, we statistically study the evolution of the sunspots and the magnetic fields in the source region of 20 flare events. This investigation will help us understand the storage and release of the magnetic energy associated with the flares. The criteria for the data selection and the methods of the data analysis are described in Section 2. We present the results and a brief discussion in Section 3.

2. DATA AND OBSERVATIONS

The *TRACE* (Handy et al. 1999) mission explores the dynamics and evolution of the solar atmosphere from the photosphere to the corona with high spatial and temporal resolution. It observes the photosphere (white light, WL), the transition region (1216, 1550, and 1600 Å), and the 1–2 MK corona (171, 195, and 284 Å). The *Hinode*/Solar Optical Telescope (SOT; Tsuneta et al. 2008) focuses on the vector magnetic field in the photosphere and on the dynamics of both the photosphere and chromosphere associated with the magnetic fields. The *Broadband Filter Imager* (*BFI*) of the SOT obtains data in the Ca II H spectral line (397 nm) and G band (430 nm) with a 2 minute cadence and a pixel size of 0.″108.

In this work, we check all 75 X-class and 513 M-class flare events[1] from 1998 May to 2009 May observed by *TRACE* and *Hinode*/SOT, and choose the event displaying one of the flare ribbons that completely sweeps across the umbra of one main sunspot of the source region. Finally, we get 7 X-class and 13 M-class events as our sample (see Table 1). For each event, we mainly use *TRACE* 1600 Å and SOT Ca II H images to study the separation of the flare ribbons. *TRACE* WL and SOT G-band images are employed to study the changes of the sunspots, and *SOHO*/Michelson Doppler Imager (MDI; Scherrer et al. 1995) observations are used to survey the evolutions of the magnetic fields in the source regions.

For the 20 events, we define the main sunspot completely swept across by the flare ribbon as the A-sunspot and its nearby opposite polarity main sunspots as the B-sunspot. In order to investigate the evolution of the flares and their source regions quantitatively, we examine a set of parameters including the rotating angle (RA_a) and rotating speed (RS_a) of the A-sunspot, the rotating angle (RA_b) and rotating speed (RS_b) of the

[1] http://hea-www.harvard.edu/trace/flare_catalog/index.html

B-sunspot, the shearing angle (A_s) and shearing speed (S_s) of the A-sunspot around the B-sunspot, the swept area (SA) of the A-sunspot umbra, the sweeping duration (SD) between the beginning of the flare and the time when the flare ribbon sweeps across the A-sunspot completely, and the sweeping speed (SS) of the flare ribbon across the A-sunspot. To describe the sunspot rotations (shear motions) conveniently, we denote that the clockwise direction is positive, and the counterclockwise one is negative.

In order to illustrate how to measure these parameters, an X3.4 class flare event that occurred in active region (AR) 10930 on 2006 December 13 is taken as an example. This has been studied by many authors. For example, Zhang et al. (2007) surveyed the rotation of the flare source region and concluded that the interaction between the fast rotating sunspot and the ephemeral regions triggered the flare, Isobe et al. (2007) studied the flare ribbons and presented that the G-band flare ribbons on sunspot umbrae showed a sharp leading edge followed by a diffuse inside, Jing et al. (2008) used the separation of the flare ribbons to study the spatial distribution of the magnetic reconnection, and Guo et al. (2008) extrapolated the three-dimensional magnetic field configuration with the optimization method. Figure 1 shows two SOT Ca II H images at the beginning and the decaying phases of the flare (see also Figure 1 in Jing et al. 2008). The solid, dotted, dashed, and dash-dotted lines display the outer edges of the southern flare ribbon at 2:20, 2:30, 2:40, and 3:40 UT, respectively. This indicates that the southern flare ribbon swept across the southern sunspots completely. According to our definition, the southern sunspots are the A-sunspot, and the northern ones are the B-sunspot. The A-sunspot is the following polarity sunspot, and the B-sunspot, consisting of one main sunspot and several small neighboring pores, is the leading polarity one. The parameters SD, SA, and SS in this event are 34 minutes, 120.1 Mm^2, and 15.1 km s^{-1}, respectively.

Figures 2(a) and (b) display two SOT G-band images that show the shear motion of the sunspots in AR 10930. The parameter A_s represents the shearing angle (denoted by the arrow in Figure 2(b)) of the A-sunspot around the B-sunspot, and reaches 28° in the two days before the occurrence of the flare. Using a linear polynomial fit to the data points, we get the average shearing speed S_s to be 0.°5 hr^{-1}. Figures 2(c) and (d) show the rotation of the A-sunspot. The parameter RA_a (marked by the arrow in Figure 2(d)) is calculated using the rotation of penumbral fibrils around the rotating center (see the circles in Figures 2(c) and (d)). Two days prior to the flare occurrence, the RA_a is −169.°5 and the rotating speed RS_a is −2.°4 hr^{-1}. The parameters RA_b and RS_b are obtained using the same methods. In this event, RA_b and RS_b are 11.°6 and 0.°5 hr^{-1}, respectively. Comparing Figure 2(c) with Figure 2(d), we notice that the A-sunspot exhibits obvious flux emergence before the occurrence of the flare.

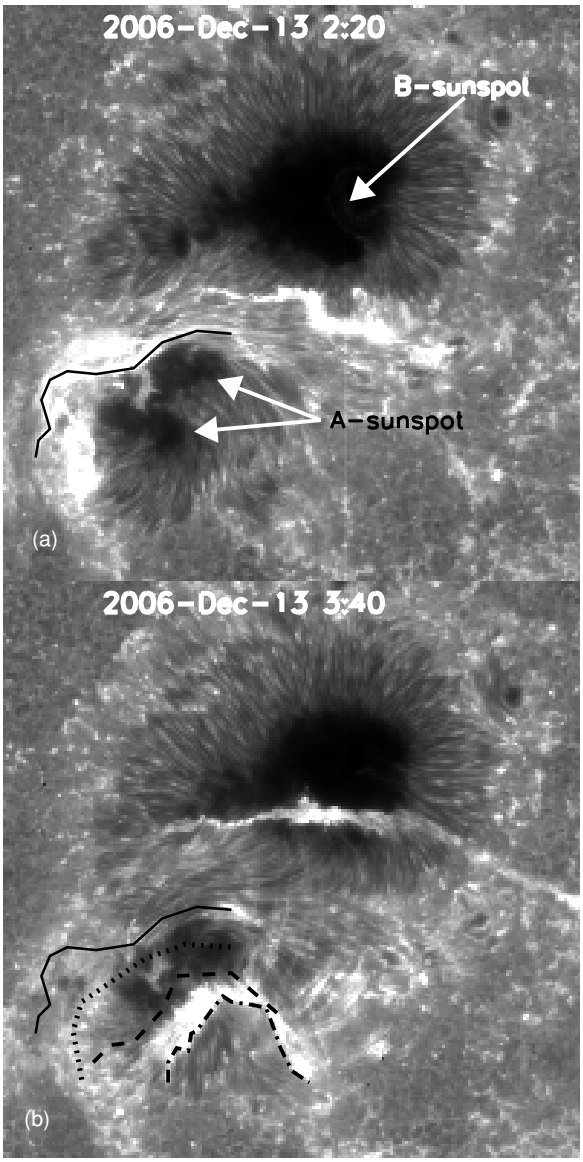

Figure 1. *Hinode*/SOT Ca II H images showing the evolution of the flare ribbons. A-sunspot and B-sunspot mark the sunspots. The curves represent the outer edges of the southern flare ribbon at different times. The field of view (FOV) is 100″ × 100″.

3. RESULTS AND DISCUSSION

In this work, nine parameters (RA_a and RS_a of the A-sunspot, RA_b and RS_b of the B-sunspot, A_s and S_s of the shear motion, SA of the A-sunspot, SD and SS of the flare ribbon) are considered to characterize the phenomenon of the flare ribbon sweeping across the A-sunspot completely. They are listed in Table 1.

Among all 75 X-class and 513 M-class flare events observed by *TRACE* and *Hinode*/SOT, 7 X-class, and 13 M-class cases illustrate that one of the flare ribbons completely sweeps across the A-sunspot, possessing 9.3% and 2.5%, respectively. In these 20 cases, the A-sunspot is the following polarity sunspot in 18 (90%) cases, and displays new emergence in 13 (65%) cases. The A-sunspot rotates in all cases, and the B-sunspot rotates in 19 (95%) cases. Among these 19 cases, the rotating directions of the B-sunspot are consistent with those of the A-sunspot in 12 cases, occupying 63%. Two days prior to the occurrence of the flare, the total rotating angles of the A-sunspot and B-sunspot in all events range from 118° to 315°, and the average value is 193°. The rotating speeds range from 0.2 to 10.°6 hr^{-1}, with an average value of 3.°2 hr^{-1}. Except for one flare event in which the B-sunspot appears as a diffusive network region, 19 cases show that the B-sunspot is relatively simple, consisting of either a main sunspot or a main sunspot and several small neighboring sunspots (pores). All the 19 events exhibit shear motions of the sunspots, and the shearing directions of 14 (74%) cases are opposite to the rotating directions of the A-sunspot. The A_ss are from 7° to 71°, with an average value of 28.°5, and the S_ss, range from 0.°2 hr^{-1} to 3.°3 hr^{-1}, with an average value of 0.°9 hr^{-1} two days before the flare occurrence.

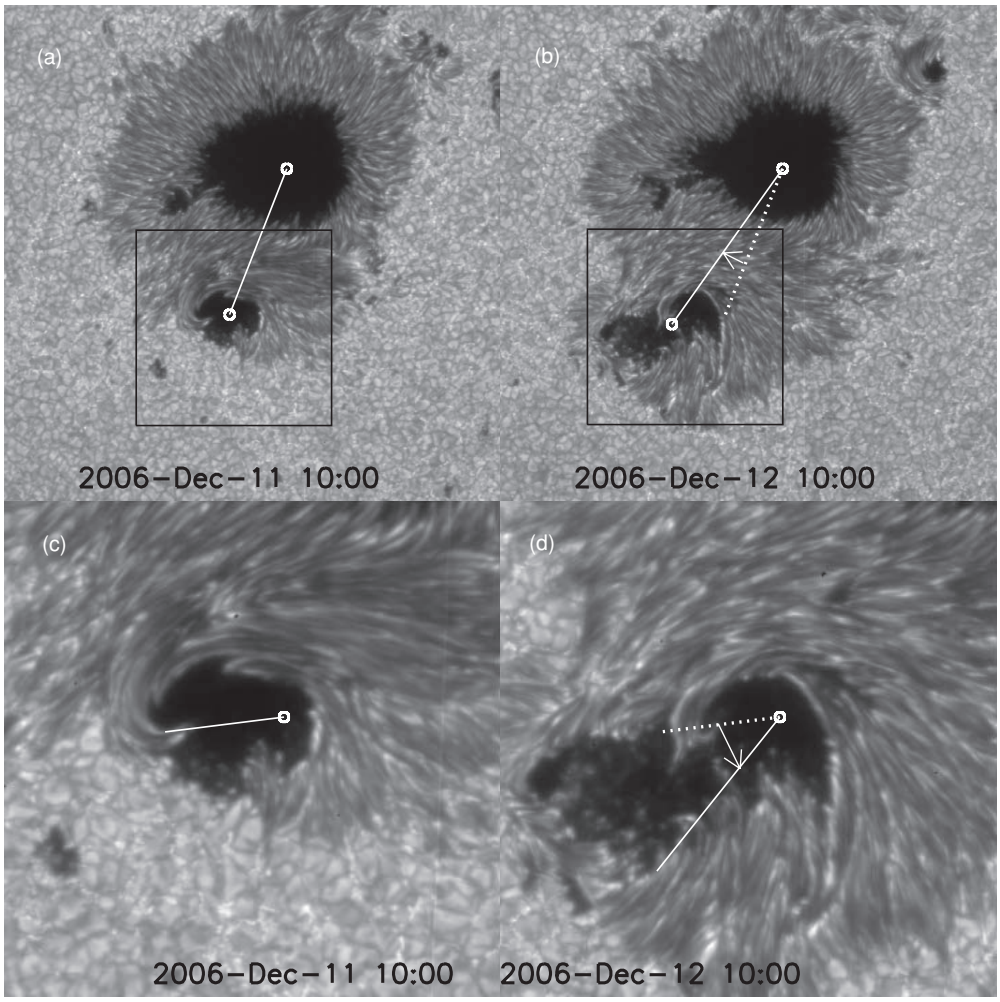

Figure 2. (a) and (b): Two *Hinode*/SOT G-band images displaying the shear motion of the sunspots. The FOV is 100″ × 100″. The circles show the center of gravity of the A-sunspot and the B-sunspot. The solid lines connect the circles. The dotted line in (b) is a copy of the solid line in (a). The arrow in (b) shows the shearing angle. The squares in (a) and (b) denote the FOV in (c) and (d), respectively. (c) and (d): Two *Hinode*/SOT G-band images showing the rotation of penumbral fibrils around the rotating center (circles; see also Zhang et al. 2007). The solid lines connect the rotating center and the penumbral fibrils. The dotted line in (d) is a duplicate of the solid line in (c). The arrow in (d) marks the rotating angle. The FOV is 40″ × 40″.

Table 1
The 20 Flare Events and Their Corresponding Nine Parameters

Date	Flare	RA_a (°)	RS_a (° hr^{-1})	RA_b (°)	RS_b (° hr^{-1})	A_s (°)	S_s (° hr^{-1})	SA (Mm^2)	SD (min)	SS (km s^{-1})
1998 Aug 23	M2.2	193.4	4	−121.9	−2	27.3	0.6	18.1	28	2.1
2000 Feb 8	M1.3	−43.1	−4.1	−98.8	−9.5	17.9	1.9	35.2	28	4.7
2000 Jun 10	M5.2	−118.1	−2.4	...	...	...	...	32.6	22.6	4.4
2000 Jun 23	M2.6	−197.5	−10.6	77	3.6	−30.1	−1.6	12.5	8.8	9.4
2001 Jan 20	M7.7	−52.1	−3	−129.1	−7.4	11.3	0.6	51.9	45	2.2
2001 Apr 9	M7.9	70.2	1.4	56.4	1.1	−34.9	−0.7	104.4	36.1	6.5
2001 Apr 11	M2.3	80.8	1.4	70.8	1.4	−35	−0.7	64.4	37.7	3.6
2001 Apr 12	X2.0	158.1	3.5	50.1	1.1	−31	−0.7	85.9	52	3.3
2001 May 12	M3.0	91.9	4.7	29.5	1.3	71.3	3.3	13.8	50.3	9.2
2002 Jul 29	M4.7	−122.4	−2.7	69.3	1.3	36	0.9	28.8	50.4	2.6
2003 Mar 18	X1.5	76.7	1.7	48.3	1	−47.4	−1	37.1	25	2.7
2003 May 29	X1.2	−173.6	−8.1	−128.6	−6.1	−24.2	−1.1	39.1	17.4	8.5
2004 Apr 6	M2.4	123.7	2.6	154.9	2.8	−60.9	−1.1	47.5	39.2	4.1
2004 Jul 20	M8.6	81.4	2.2	77.4	2.2	−7.1	−0.2	26.4	10.3	16.8
2005 Jul 9	M2.8	−96.6	−2	−85.5	−0.8	22.6	0.4	30.6	27.3	5.9
2005 Aug 1	M1.0	84.7	1.6	−78	−1.5	16.4	0.4	31.4	67	1.6
2005 Sep 9	X6.2	36.6	1.2	101	4.3	−10.5	−0.4	72.5	58.5	1.8
2006 Dec 6	X6.5	−213.9	−9.9	11.6	0.5	14.5	0.5	34.7	18.2	7.3
2006 Dec 13	X3.4	−169.5	−2.4	12.9	0.2	28	0.5	120.1	34	15.1
2006 Dec 14	X1.5	−257.4	−5.1	15.6	0.3	15.4	0.3	81.1	53.4	7.5

Table 2
The Statistical Results of the 20 Flare Events in the Sample

Character	Rotation			Shear	Motion	A Flux	A Polarity
Type	A	B	A=B	S	S≠A	Emergency	Following
Numbers	20	19	12	19	14	13	18
Percentage	100%	95%	63%	95%	74%	65%	90%

Notes. A denotes the A-sunspot, B the B-sunspot, and S the shear motion. A=B means that the rotating directions of the A-sunspot and B-sunspot are the same, and S≠A means that the shearing direction is opposite to the rotating direction of the A-sunspot.

The SAs, SDs, and SSs are 12.5–120.1 Mm^2, 8–67 minutes, and 1.6–16.8 km s^{-1}, with an average value of 48.4 Mm^2, 35.2 minutes, and 6 km s^{-1}, respectively. All the statistical results are listed in Table 2.

Only 20 (3.4%) flare events among 588 display flare ribbons that sweep across sunspots completely, indicating that this phenomenon is few and far between. The A-sunspot is the following polarity sunspot in 90% of the cases, showing that it is easier for the following polarity sunspots than the leading polarity ones to be completely swept across by the flare ribbons.

Flares are common phenomena and quickly release magnetic energy stored in the corona in a short time. The manners of storing the magnetic energy include rotation and shear motion of sunspots, magnetic flux emergence, etc. Rotating sunspots have already been observed for one century (Evershed 1910; Maltby 1964; Gopasyuk 1965). Stenflo (1969) suggested that sunspot rotation may be involved with the buildup of magnetic energy, which is later released by a flare. Régnier & Canfield (2006) presented that the slow rotation of the sunspot in NOAA Active Region 8210 enables the storage of magnetic energy and allows for the release of magnetic energy as flares. Recently, more and more observations provided evidence that the rotating sunspot is involved in large flare activity (e.g., Zhang et al. 2007; Yan & Qu 2007). In our sample, all the flare events are associated with the sunspot rotation, consistent with the results mentioned above. The rotating directions of the A-sunspot and the B-sunspot are the same in 63% of the cases, which is identical with Yan et al. (2008) who proposed that the two sunspots with the same rotating direction have higher flare productivity than those with opposite rotating directions, and that this scenario makes it easier to store magnetic energy and increase the helicity of the flux tube. Furthermore, we find shear motions of the A-sunspot around the B-sunspot in 19 cases, and the shearing directions of 74% of the cases are opposite to the rotating directions of the A-sunspot. It seems that two sunspots with the same rotating direction but opposite shearing directions accumulate magnetic energy and produce flares more easily. Brown et al. (2003) have shown that some sunspots rotate up to 200° about their umbral center, and the corresponding loops in the corona fan twist and erupt as flares. Gerrard et al. (2003) have simulated the rotation of a pore around a sunspot, and found that when the pore rotates 180° around the sunspot, the current increases rapidly as the center of the pore makes contact with the large sunspot, which could explain an observed flare. In this work, the average total rotating angles of the A-sunspot and B-sunspot is 193° two days prior to the occurrence of the flare, which corresponds to the results of Brown et al. and Gerrard et al. Schrijver et al. (2008) used nonlinear force-free modeling to show the evolution of the coronal field associated with a rotating sunspot and suggested that the flare energy comes from an emerging twisted flux rope. In this Letter, 13 (65%) flare events display new flux emergence that is identical with the simulation of Schrijver et al. The parameter SA may represent the magnetic flux included in the flare. We use the average swept area of 48.4 Mm^2 and the magnetic field strength of 1500 G to estimate the magnetic flux involved in a flare, and get a value of 7.3×10^{20} Mx.

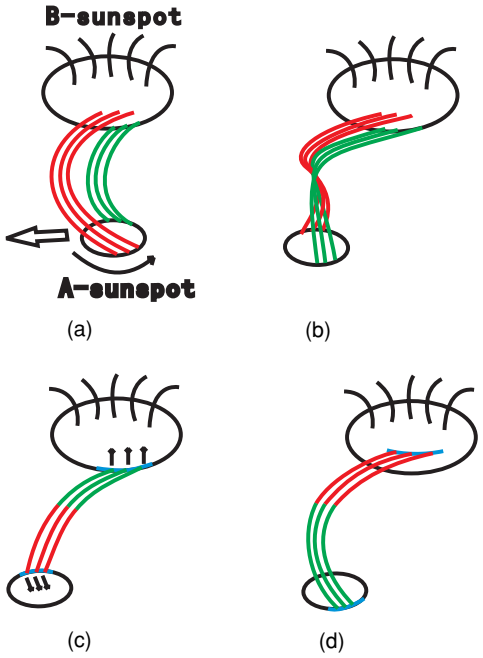

Figure 3. Schematic diagrams illustrating the evolution of the magnetic field lines in the source region of the flare. The ellipses show the sunspots (the A-sunspot and B-sunspot), and the curves show the magnetic field lines. The thin arrow in (a) represents the rotating direction, and the hollow one in (a) represents the shearing direction. The blue ribbons in (c) and (d) represent the flare ribbons, and the arrows in (c) represent the separating directions of the flare ribbons.

The magnetic field structures and sunspot evolution may respond to the phenomenon that the flare ribbons sweep across the sunspots. In our study, the B-sunspot is relatively simple, which means that almost all the magnetic field lines of the A-sunspot may connect with the B-sunspot. The rotation and shear motions of the sunspots twist the magnetic field lines above the source region together, accumulate the magnetic energy, and inject the emerging twisted flux into the corona. Then, sigmoids/Ω loops erupt as flares and coronal mass ejections (Canfield et al. 1999; Pevtsov 2002; Régnier & Amari 2004). In the process of the flare, all the twisted field lines of the A-sunspot are rearranged by the successive magnetic reconnection. That is why we observe that the flare ribbon sweeps across the A-sunspot completely.

Based on the statistical results, we use schematic diagrams to illustrate the evolution of the magnetic field lines of the A-sunspot. Figure 3(a) shows the magnetic configuration of the AR two days before the flare, showing all the field lines (the green and the red lines) of the A-sunspot connecting with the B-sunspot (see also Guo et al. 2008). In the following two days, the rotation (see the thin arrow) and shear motion of the sunspots (see the hollow arrow) twist the field lines of the A-sunspot together, inject twisted flux into the corona, form complicated magnetic topology in the AR (see Figure 3(b)), and accumulate the magnetic energy. When the magnetic energy exceeds a critical value, e.g., the rotating angle is beyond 180°, the twisted field lines reconnect, the magnetic energy is released, and the flare begins. At the beginning of the flare, the lower field lines reconnect (the red and green lines in Figure 3(c)),

and then the lower post-flare loops appear. The footpoints of these post-flare loops form the flare ribbons (the blue lines in Figure 3(c)). Therefore, we find that the flare ribbons first appear near the magnetic neutral lines of the two sunspots. As the magnetic reconnection continues and the reconnection points move upward, the flare ribbons separate (see the arrows in Figure 3(c)) from each other. As a result, we note that the flare ribbons sweep the umbrae of the sunspots. Figure 3(d) shows the reconnected field lines (the green and red lines) and the flare ribbons (the blue lines) in the decaying phase of the flare. During the flare, all the field lines of the A-sunspot are involved in the process of magnetic reconnection. Therefore, we find that the flare ribbons sweep across the A-sunspot completely.

However, statistics is just one aspect. More observations, simulations, and theoretical studies are needed in order to fully understand the nature of this phenomenon. An analysis of a typical example of high-resolution images and magnetograms compared with simulations is planned.

The authors are indebted to the *TRACE*, the *Hinode*, and the *SOHO*/MDI teams for providing the data. The work is supported by the National Natural Science Foundations of China (G40890161, 10703007, 10873020, 10603008, 40674081, and 10733020), the CAS Project KJCX2-YW-T04, the National Basic Research Program of China under grant G2006CB806303, and the Young Researcher Grant of the National Astronomical Observatory, the Chinese Academy of Sciences.

REFERENCES

Asai, A., Yokoyama, T., Shimojo, M., & Shibata, K. 2004, ApJ, 605, L77
Brown, D. S., et al. 2003, Sol. Phys., 216, 79
Canfield, R. C., Hudson, H. S., & McKenzie, D. E. 1999, Geophys. Res. Lett., 26, 627
Carmichael, H. 1964, in The Physics of Solar Physics, ed. W. N. Hess (NASA SP-50; Washington, DC: NASA), 451
Evershed, J. 1910, MNRAS, 70, 217
Gerrard, C. L., Brown, D. S., Mellor, C., Arber, T. D., & Hood, A. W. 2003, Sol. Phys., 213, 39
Gopasyuk, S. I. 1965, Izv. Krym. Astrofiz. Obs., 33, 100
Guo, Y., Ding, M. D., Wiegelmann, T., & Li, H. 2008, ApJ, 679, 1629
Handy, B. N., et al. 1999, Sol. Phys., 187, 229
Hirayama, T. 1974, Sol. Phys., 34, 323
Isobe, H., et al. 2002, ApJ, 566, 528
Isobe, H., et al. 2007, PASJ, 59, S807
Jing, J., Chae, J. C., & Wang, H. M. 2008, ApJ, 672, L73
Kopp, R. A., & Pneuman, G. W. 1976, Sol. Phys., 50, 85
Li, L. P., & Zhang, J. 2009a, ApJ, 690, 347
Li, L. P., & Zhang, J. 2009b, ApJ, 703, 877
Maltby, P. 1964, Astrophys. Nor., 8, 205
Pevtsov, A. A. 2002, Sol. Phys., 207, 111
Qiu, J., Lee, J., Gary, D. E., & Wang, H. M. 2002, ApJ, 565, 1335
Régnier, S., & Amari, T. 2004, A&A, 425, 345
Régnier, S., & Canfield, R. C. 2006, A&A, 451, 319
Scherrer, P. H., et al. 1995, Sol. Phys., 162, 129
Schrijver, C. J., et al. 2008, ApJ, 675, 1637
Stenflo, J. O. 1969, Sol. Phys., 8, 115
Sturrock, P. A. 1966, Nature, 211, 695
Tsuneta, S., et al. 2008, Sol. Phys., 249, 167
Yan, X. L., & Qu, Z. Q. 2007, A&A, 468, 1083
Yan, X. L., Qu, Z. Q., & Kong, D. F. 2008, MNRAS, 391, 1887
Zhang, J., Li, L. P., & Song, Q. 2007, ApJ, 662, L35